

Dalton Transactions

Accepted Manuscript



This is an *Accepted Manuscript*, which has been through the Royal Society of Chemistry peer review process and has been accepted for publication.

Accepted Manuscripts are published online shortly after acceptance, before technical editing, formatting and proof reading. Using this free service, authors can make their results available to the community, in citable form, before we publish the edited article. We will replace this *Accepted Manuscript* with the edited and formatted *Advance Article* as soon as it is available.

You can find more information about *Accepted Manuscripts* in the [Information for Authors](#).

Please note that technical editing may introduce minor changes to the text and/or graphics, which may alter content. The journal's standard [Terms & Conditions](#) and the [Ethical guidelines](#) still apply. In no event shall the Royal Society of Chemistry be held responsible for any errors or omissions in this *Accepted Manuscript* or any consequences arising from the use of any information it contains.

Cite this: DOI: 10.1039/c0xx00000x

www.rsc.org/xxxxxx

ARTICLE TYPE

An open chain carboxyethyltin functionalized sandwich-type tungstophosphate based on trivacant Dawson subunit: synthesis, characterization and properties

Jian-Ping Bai,^a Fang Su,^{a,b} Hao-Tian Zhu,^a Hang Sun,^a Lan-Cui Zhang,^{*a} Mei-Ying Liu,^a Wan-Sheng You^{*a} and Zai-Ming Zhu^{*a}

Received (in XXX, XXX) Xth XXXXXXXXX 20XX, Accepted Xth XXXXXXXXX 20XX

DOI: 10.1039/b000000x

A Dawson sandwich-type polyoxometalate $\{C(NH_2)_3\}_{12}H_4[\alpha\beta\beta\alpha-\{Sn(C_3H_4O_2)_2Mn_2(P_2W_{15}O_{56})_2\}]\cdot 22H_2O$ (Abbreviated as **SnR-Mn-P₂W₁₅**), functionalized by open chain carboxyethyltin groups was first prepared in aqueous solution under conventional reaction conditions, and structurally characterized by physico-chemical and spectroscopic methods. Single crystal X-ray diffraction analysis revealed that two Mn^{2+} cations and two $[Sn(CH_2CH_2COO)]^{2+}$ groups were located in the internal and external positions in the so-called equatorial region of **SnR-Mn-P₂W₁₅**, respectively. Intriguingly, two exposed carboxyl groups come into being stretching-arm brackets, which provide a favorable structure for potential further functionalization. The electrocatalytic studies of **SnR-Mn-P₂W₁₅** towards the reduction of hydrogen peroxide and nitrite were performed. Additionally, its acid catalysis and oxidation catalysis activities in organic synthesis were also investigated.

Introduction

Polyoxometalates (POMs), as an extended family of anionic metal-oxo clusters, have received wide-ranging and painstaking researches not only due to their unparalleled structural styles and fascinating physicochemical properties including alterable shape, size, oxygen-rich surface and high-negative charge but also due to extreme versatility and particularity in application areas of medicine, materials science, catalytic chemistry, magnetochemistry and photoelectrochemistry.¹ Theoretical and experimental studies give a clear view that sandwich-type POMs incorporated metals in the central core are of great enthusiasm since they can be used as secondary building blocks to expand the architectures of POMs. The previous work discovered that lacunary Keggin anion $[XW_9O_{34}]^{n-}$ (X = As(V), P(V), Si(IV)...) fragments or Wells-Dawson $[X_2W_{15}O_{56}]^{12-}$ (X = As(V), P(V)) ions could be easily to obtain such transition-metal-decorated sandwich-type POM clusters.² Pope's group reported the first example of three phenyltin-containing tungstophosphate $[(PhSnOH)_3(PW_9O_{34})_2]^{12-}$ which was synthesized by routine method in 1994.³ Frequently novel polyoxoanions containing organotin groups were found, which provided a platform for the development of inorganic-organic hybrids with special properties and potential functionalities.⁴ Based on these pioneering work, several research teams turned attention to the synthesis and characterization of estertin/carboxyethyltin-modified polyoxometalates.⁵ Nevertheless, a few crystal structures were obtained, which can be traced to the fact that the mechanism of formation of POM-estertin/carboxyethyltin derivatives is not well understood and the isolation in aqueous medium is more difficult.

To date, some crystal examples of sandwich-type POMs beautified by carboxyethyltin were reported by our team,^{1d,6} which are based on trivacant Keggin unit, but no single crystalline of carboxyethyltin functionalized Dawson sandwich-type POM was obtained. In consideration of hypotoxicity and favorable heat endurance of eatertin or carboxyethyltin compound,⁷ along with the trivacant Dawson monomer $[P_2W_{15}O_{56}]^{12-}$ (Abbreviated as **P₂W₁₅**) providing more active sites for further functionalization,⁸ we attempted to optimize the performance of POM precursor by grafting transition metal (TM) cations and organometallic (OM) groups onto the **P₂W₁₅** skeleton. Within this context, we described the synthesis and characterization of a new POM-estertin derivative, **SnR-Mn-P₂W₁₅**, the first single crystal Dawson sandwich-type POM functionalized by open chain carboxyethyltin. The electrocatalytic activities of **SnR-Mn-P₂W₁₅** towards the reduction of hydrogen peroxide and nitrite were explored, besides, the catalytic activities in the synthesis of cyclohexanone ethylene ketal and the oxidation of cyclohexanol to cyclohexanone were also evaluated, respectively.

Experimental

Reagents and materials

All reagents were obtained and used as received from commercial sources without further purification. The parent POMs, *i.e.* α -**P₂W₁₅** and the sandwich-type tungstophosphate $Na_8H_8[\alpha\beta\beta\alpha-\{Mn_4(H_2O)_2(P_2W_{15}O_{56})_2\}]\cdot 61H_2O$ (Abbreviated as **Mn-P₂W₁₅**) were prepared by the reported procedures,⁹ the organotin precursor $Cl_3SnCH_2CH_2COOCH_3$ was synthesized by the literature,¹⁰ and

Table 1 Crystal and Refinement Data for **SnR-Mn-P₂W₁₅**

Compound	SnR-Mn-P₂W₁₅
Formula	C ₁₈ H ₁₂₈ O ₁₃₈ N ₃₆ Mn ₂ Sn ₂ P ₄ W ₃₀
Formula weight	9044.20
<i>T</i> /K	296(2)
Wavelength/Å	0.71073
Crystal system	Monoclinic
Space group	<i>P</i> 2(1)/ <i>n</i>
<i>a</i> , <i>b</i> , <i>c</i> /Å	13.3516(9), 32.355(2) 19.0312(13)
<i>α</i> , <i>β</i> , <i>γ</i> /°	90.00, 94.100(1), 90.00
<i>V</i> /Å ³ , <i>Z</i>	8200.3(10), 2
<i>D_c</i> /g cm ⁻³ , <i>F</i> ₀₀₀	3.663, 8044
GOF	1.051
Reflections collected	41351
<i>R</i> _{int}	0.0594
<i>θ</i> Range(°)	1.65 to 25.00
<i>R</i> ₁ (<i>I</i> > 2σ(<i>I</i>)) ^a	0.0455
<i>wR</i> ₂ (all data) ^a	0.1188

$$^a R_1 = \frac{\sum ||F_o| - |F_c||}{\sum |F_o|}; wR_2 = \frac{\sum [w(F_o^2 - F_c^2)^2]}{\sum [w(F_o^2)]^{1/2}}$$

Electrocatalytic activities. The electrocatalytic activities of **SnR-Mn-P₂W₁₅** and the parent compounds towards the reduction of hydrogen peroxide and nitrite were studied at room temperature in the potential range of +0.2 to -1.0 V. The dosages of H₂O₂ and NaNO₂ were 0 to 2 and 0 to 4 mmol, respectively. Their electrocatalytic activities can be evaluated by peak current changes in the CV curves.

Acid-catalyzed synthesis of cyclohexanone ethylene ketal. General procedure for the catalytic synthesis is followed: the catalyst was added to a mixture of cyclohexanone, glycol and cyclohexane (10 mL) in a 50 mL three-necked round-bottom flask fitted with a Dean-Stark apparatus to carry off the water continuously from the reaction system. The as-prepared catalyst catalyzed reaction is a heterogeneous process, after the reaction finished, the catalyst can be separated easily from the reaction mixture by decantation. The products obtained were characterized by gas chromatography.

Catalytic oxidation of cyclohexanol to cyclohexanone. In a typical procedure, 0.015 mmol **SnR-Mn-P₂W₁₅** was added to the mixture of 0.092 mol cyclohexanol and 10 mL acetonitrile remained in a three-necked round-bottom flask equipped with a reflux condenser, which was accompanied by adding 20 mL H₂O₂ dropwise. After 2.5 h, distillation was operated in order to remove the solvent acetonitrile, the residue was decanted to a separating funnel to received organic phase containing product. The products obtained were also analyzed by gas chromatography.

Repeating the above experiment under the same conditions except that **SnR-Mn-P₂W₁₅** was replaced by the parent POMs **P₂W₁₅** and **Mn-P₂W₁₅**, and raw materials MnCl₂ and Cl₃SnCH₂CH₂COOCH₃, respectively.

90 Results and discussion

Synthesis

At the mention of the preparation of inorganic-organic hybrids, for example, polyoxometalate estertin derivatives, it is hard to control and predict the resultant structures owing to the fierce competition between the inorganic and organic metals. In addition, it is hard to isolate POM estertin derivatives from the

both of them were characterized by IR spectroscopy. C, H and N elemental analyses were performed on a Vario Elcube elemental analyzer, and P, Sn, Mn and W were analyzed on a Prodigy XP emission spectrometer. The IR spectrum was recorded using KBr pellets on a Bruker AXS TENSOR-27 FTIR spectrometer in the range of 4000-400 cm⁻¹. TG analysis was performed on a Pyris Diamond TG-DTA thermal analyzer at a heating rate of 10 °C min⁻¹ in an air atmosphere. Single crystal X-ray diffraction data was collected on a Bruker Smart APEX II X-diffractometer equipped with graphite-monochromated Mo Kα radiation (*λ* = 0.71073 Å). X-ray powder diffraction (XRPD) data was collected on a Bruker AXS D8 Advance diffractometer using Cu Kα radiation (*λ* = 1.5418 Å) in the 2*θ* range of 5-60 ° with a step size of 0.02 °. UV spectra were performed on a Lambda 35 UV-Visible spectrophotometer. NMR spectra were recorded at room temperature with a 500 MHz Bruker AVANCE 500 spectrometer. An inner tube containing D₂O was used as an instrumental lock. Phosphorus and tin chemical shifts were referenced to 85% H₃PO₄ and (CH₃)₄Sn, respectively. A CHI 604B electrochemical work station was used to control the electrochemical measurements and collect data. A conventional three electrode system was used. The working electrode was a glassy carbon electrode. Ag/AgCl was used as a reference electrode and a platinum wire as a counter electrode.

25 Synthesis of SnR-Mn-P₂W₁₅

Cl₃SnCH₂CH₂COOCH₃ (0.1 g, 0.32 mmol) was dissolved in 30 mL of 1 mol L⁻¹ NaCl aqueous solution with vigorous stirring. Then **Mn-P₂W₁₅** (0.2 g, 0.02 mmol) was added in small portions to obtain a clear, orange solution. The resulting mixture was further stirred for 5 h at 90 °C. After cooling to ambient temperature, the insoluble material was filtered off and the clear filtrate was treated with solid KCl (0.5 g, 6.7 mmol) and 1.5 mL of 1 mol L⁻¹ C(NH₂)₃Cl aqueous solution. Slow evaporation at 50 °C led to the appearance of orange crystalline **SnR-Mn-P₂W₁₅** after about 10 days (Yield: *ca.* 37 % based on W). Elemental analysis, Found: C, 2.4; H, 1.5; N, 5.7; P, 1.4; Mn, 1.2; Sn, 2.8; W, 61.1. Calc. for C₁₈H₁₂₈O₁₃₈N₃₆Mn₂Sn₂P₄W₃₀: C, 2.4; H, 1.4; N, 5.6; P, 1.4; Mn, 1.2; Sn, 2.6; W, 61.0%. FT IR (KBr pellet), cm⁻¹: 3430(s), 3260(w), 3185(m), 2925(w), 2856(w), 1665(s), 1461(sh), 1399(m), 1096(m), 948(s), 910(m), 756(s), 602(w), 522(w), 412(w).

X-ray crystallography

The structure was solved by direct methods and refined by full-matrix least-squares fitting on *F*² using SHELXTL-97.¹¹ An empirical absorption correction was applied using the SADABS program. Crystal data and structure refinement parameters of **SnR-Mn-P₂W₁₅** are listed in Table 1. Hydrogen atoms on C/N atoms were added in calculated positions. In **SnR-Mn-P₂W₁₅**, only partial lattice water molecules can be accurately assigned from the residual electron peaks, whereas the rest were directly included in the molecular formula on the basis of the SQUEEZE calculation results, the elemental analysis and TG analysis. Selected bond lengths and angles are listed in Table S1.† Hydrogen bonds are listed in Table S2.† CCDC reference number: 1045128

Catalytic experiments

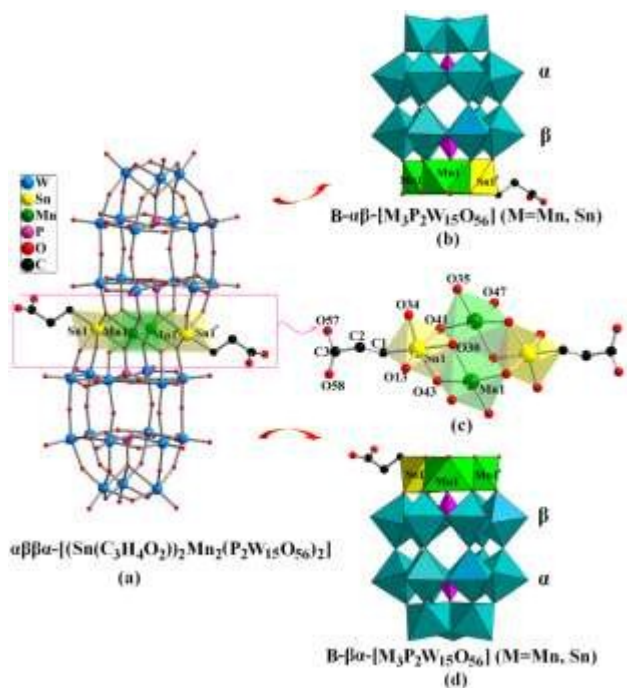


Fig. 1 The crystal structure of $\text{SnR-Mn-P}_2\text{W}_{15}$. (a) Ball-and-stick representation of the polyoxoanion of $\text{SnR-Mn-P}_2\text{W}_{15}$; (b)/(d) The Dawson trimetal-substituted POM unit in $\text{SnR-Mn-P}_2\text{W}_{15}$; (c) Mixed ball-and-stick and polyhedral representation of the $\{(\text{SnCH}_2\text{CH}_2\text{COO})_2\text{Mn}_2\text{O}_{14}\}$ fragment in $\text{SnR-Mn-P}_2\text{W}_{15}$

solution. To overcome the synthetic defects, the stepwise assembly depending on preconstructed precursors is essential. Consequently, the choice of suitable precursor is the key to obtain POM derivatives in aqueous media. The sandwich-type polyoxometalate $\text{Mn-P}_2\text{W}_{15}$ is a good candidate as an inorganic precursor based on several considerations. On the one hand, $\text{Mn-P}_2\text{W}_{15}$ is obtained easily by a mature method (the reaction of Mn^{2+} cation and P_2W_{15} in an appropriate solution), on the other hand, the polyoxoanion of $\text{Mn-P}_2\text{W}_{15}$ possesses higher overall charge than those of the sandwich-type Keggin architectures, which improves the coordination tendency with organotin groups and leads to the novel carboxyethyltin modified POMs with ease. We have tried to use carboxyethyltin as an organic precursor, but failed to obtain high-quality perfect crystalline products, and it was too difficult to isolate the products from the reaction system as well. Estertin was found to be the best organic precursor for the crystal growth of such POM-organotin hybrid compounds so far.

25 Structural analysis

Single-crystal X-ray diffraction analysis reveals that $\text{SnR-Mn-P}_2\text{W}_{15}$ crystallizes in the monoclinic space group P2(1)/n . $\text{SnR-Mn-P}_2\text{W}_{15}$ can be described structurally as the well-known sandwich-type structure (Fig. 1a). The structural skeleton of the compound can be divided into three portions which separately are two Dawson POM subunits and one central organotin-transition metal group. As shown in Fig. 1b and 1d, two trimetal-substituted Dawson POM subunits display classical $\text{B-}\alpha\beta\text{-}$ and $\text{B-}\beta\alpha\text{-}$ configuration, which can be depicted by a group of three mutually corner-shared WO_6 octahedra.^{2a} Two $[\text{Sn}(\text{CH}_2)_2\text{COO}]^{2+}$ segments and two Mn^{2+} cations are sandwiched between two

trivalent P_2W_{15} moieties in external and internal locations, respectively, which are surrounded by twelve $[\text{C}(\text{NH}_2)_3]^+$ cations and twenty-two lattice water molecules (Fig. S1†). In the polyoxoanion of $\text{SnR-Mn-P}_2\text{W}_{15}$, each $\alpha\text{-P}_2\text{W}_{15}$ unit supplies seven oxygen atoms (one central and six terminal oxygen atoms) that are able to coordinate with two edge-sharing MnO_6 octahedra as well as two $[\text{Sn}(\text{CH}_2)_2\text{COO}]^{2+}$ units. Sn1 is hexa-coordinated with five oxygen atoms (O13, O30, O34, O41 and O43) and one carbon atom (C1) derived from carboxyethyl group (Fig. 1c and S2†). The Sn–O bond distances are 2.069(11)–2.223(11) Å, while the Sn–C bond distance is 2.16(2) Å. The bond lengths of Mn–O and W–O are in the range of 2.043(11)–2.301(12) Å and 1.691(12)–2.412(11) Å (Table S1†), respectively. The adjacent sandwich-type polyoxoanions are accumulated to form a 3D supramolecular framework by hydrogen bonds ($\text{N-H}\cdots\text{O}/\text{O/W}$ 2.82(3)–3.37(2) Å, Table S2†) between guanidine cations and the polyoxoanions or water molecules, along with the electrostatic forces exist in $[\text{C}(\text{NH}_2)_3]^+$ cations and the polyoxoanions (Fig. S3†). In $\text{SnR-Mn-P}_2\text{W}_{15}$, bond valence sum (BVS) calculations show that all W, Sn, Mn and P atoms are in the +6, +4, +2 and +5 oxidation states, and all O atoms are 2, respectively, which indicates that none of O atoms is protonated. In virtue of isolation from weak-acidic aqueous solution for this compound, thus four protons are attached to the counter cations part to compensate charge balance.¹² The phenomenon of the estertin precursor $[\text{Sn}(\text{CH}_2)_2\text{COOCH}_3]^{3+}$ hydrolyzing into carboxyethyltin $[\text{Sn}(\text{CH}_2)_2\text{COOH}]^{3+}$ occurred during the reaction course and was similar to those occurred in our previous work.^{1d,6} In particular, the Sn–O bond once existed in a cyclic estertin precursor was broken, that is, the five-membered ring was opened, which led to the formation of an open chain structure instead of cyclic carboxyethyltin, as shown in Scheme S1.† The exposed carboxyl group ($-\text{COO}^-$) may advantageously be further functionalized. Historically, the title compound represents the first example of trivalent Dawson-type POM derivative modified by the open chain carboxyethyltin.

Characterizations

IR spectroscopy. As shown in Fig. S4,† the feature peaks between 1096–756 cm^{-1} can be attributed to the characteristic vibrations of POM skeleton, the bands at 1096, 948, 910, 756 cm^{-1} are ascribed to the $\nu(\text{P-O}_a)$, $\nu(\text{W=O}_d)$, $\nu(\text{W-O}_b)$ and $\nu(\text{W-O}_c)$ (O_a , O_b/O_c and O_d represent tetrahedral, bridging and terminal O atoms), respectively.^{8a} The appearance of 421 cm^{-1} peak can be regarded as symmetric vibration of Sn–C bond. The observed overlapped peak at 522 cm^{-1} may be caused by $\nu(\text{Mn-O})$ and antisymmetric vibration of Sn–C bond.¹³ The broad band of lattice water molecules is located at 3430 cm^{-1} . The peaks of $\nu(\text{N-H})$ lie in 3260–3185 cm^{-1} . Peaks at 2925 and 2856 cm^{-1} are ascribed to the stretching vibration of organic group $-\text{CH}_2-$, and its bending vibration band is observed at 1461 cm^{-1} ,¹⁴ while the sharp peaks at 1665 and 1399 cm^{-1} are attributed to the stretching vibration of $-\text{COO}^-$. All the results indicate the presence of carboxyethyltin group and POM framework in $\text{SnR-Mn-P}_2\text{W}_{15}$, which is in good agreement with single-crystal structural analysis.

Thermal analysis. To investigate the thermal stability of $\text{SnR-Mn-P}_2\text{W}_{15}$, TG analysis was carried out and shown in Fig. S5a.† A continuous weight loss process occurred in temperature range

of 35-730 °C. The first weight loss at 35-187 °C is 4.38% (calcd.

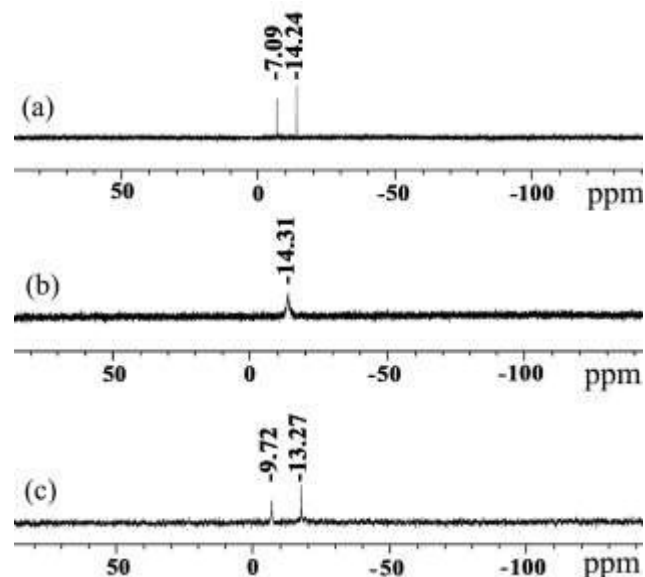


Fig. 2 The ^{31}P NMR ($\text{D}_2\text{O}/85\%\text{H}_3\text{PO}_4$) spectra of (a) monomer P_2W_{15} , (b) starting material $\text{Mn-P}_2\text{W}_{15}$ and (c) $\text{SnR-Mn-P}_2\text{W}_{15}$

4.38%), corresponding to the loss of all lattice water molecules. The observed continuous weight loss of 9.69% (calcd. 9.59%) in the temperature range of 187 to 431 °C attributes to the removal of twelve $[\text{C}(\text{NH}_2)_3]^+$ organic cations and four H^+ , as well as two $\text{C}_3\text{H}_4\text{O}_2$ groups.^{14,15} Additionally, the compound continuously lost weight at temperatures higher than 431 °C, which is mainly assigned to the loss of phosphorus oxide etc. species that are easily to sublime.^{5c,6d} This result suggests that the thermal stability of $\text{SnR-Mn-P}_2\text{W}_{15}$ is lower than those of the substituted monomer compound and its sandwich-type parent compound $\text{Mn-P}_2\text{W}_{15}$ (Fig. S5b†). Nevertheless, after 730 °C the curve rising slightly, which may be caused by the oxidation process of tin in the air ambience.^{14,15,16} It can be found that the results of the TG analysis are basically in agreement with those structure determinations and the analysis of variable-temperature IR spectra (Fig. S6†).

X-ray powder diffraction. The XRPD patterns for experimental and simulated results of $\text{SnR-Mn-P}_2\text{W}_{15}$ are presented in Fig. S7.† The diffraction peaks of two patterns match well, indicating the good phase purity for this compound. The difference of intensity is probably due to the variation in preferred orientation of the powder sample during collection of the experimental XRPD pattern.

UV-visible spectroscopy. As shown in Fig. S8,† the UV-visible absorption spectrum of $\text{SnR-Mn-P}_2\text{W}_{15}$ reveals the same features as the parent compound $\text{Mn-P}_2\text{W}_{15}$, it also exhibits a broad band in the near-UV region. The absorbance at ca. 275 nm in 1 mol L^{-1} NaCl for $\text{Mn-P}_2\text{W}_{15}$ red shifts to 285 nm and increases when organotin groups are introduced to $\text{Mn-P}_2\text{W}_{15}$. The absorption bands are attributed to the oxygen to metal ($\text{O} \rightarrow \text{W}$) charge transfer (LMCT) bands.¹⁷

NMR analysis. ^{31}P NMR ($\text{D}_2\text{O}/\text{PO}_4^{3-}$) for $\text{SnR-Mn-P}_2\text{W}_{15}$ emerged with two intense peaks: $\delta = -9.72, -13.27$ ppm (Fig. 2c), which is consistent with the structural feature peaks of P_2W_{15} located at $\delta = -7.09, -14.24$ ppm (Fig. 2a), indicating that

40 phosphorous atoms exist in two diverse chemical environments. While for the starting material $\text{Mn-P}_2\text{W}_{15}$, the ^{31}P NMR signals

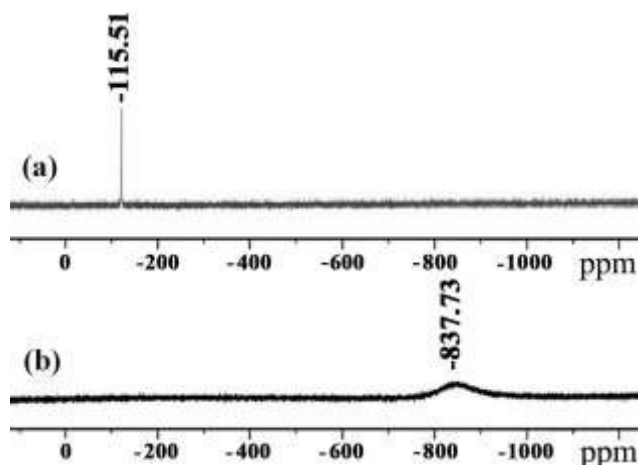
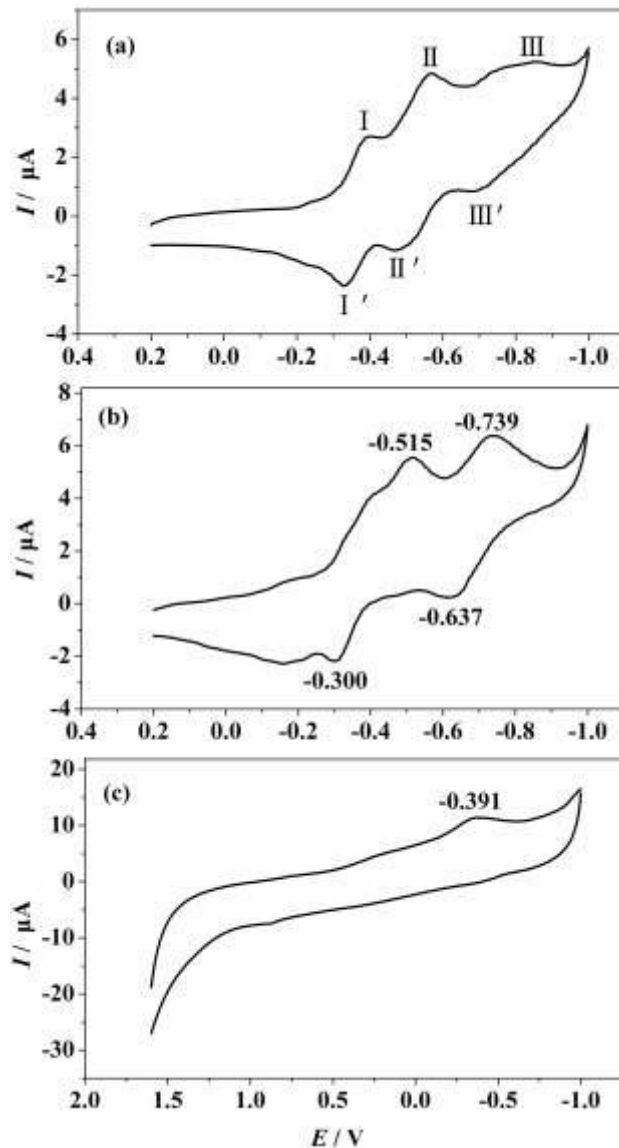


Fig. 3 The ^{119}Sn NMR spectra of (a) $\text{Cl}_3\text{SnCH}_2\text{CH}_2\text{COOCH}_3$ $\text{CDCl}_3/(\text{CH}_3)_4\text{Sn}$ and (b) $\text{SnR-Mn-P}_2\text{W}_{15}$ ($\text{D}_2\text{O}/(\text{CH}_3)_4\text{Sn}$)



45

Fig. 4 Cyclic voltammograms of **SnR-Mn-P₂W₁₅** (a), **Mn-P₂W₁₅** (b) and **Cl₃Sn(CH₂)₂COOCH₃** (c) in 1 mol L⁻¹ Na₂SO₄-H₂SO₄ (pH = 4) aqueous solutions at the scan rate of 50 mV s⁻¹.

were broadened by four incorporated paramagnetic manganese ions.¹⁸ So, only one peak at $\delta = -14.31$ ppm (Fig. 2b) was detected. As seen in Fig. 3b, the ¹¹⁹Sn chemical shift (-837.73 ppm) of **SnR-Mn-P₂W₁₅** moved to a higher magnetic field compared with that of the origin material **Cl₃Sn(CH₂)₂COOCH₃** (-115.51 ppm, Fig. 3a), which provided a proof that the organotin group was connected to the framework of **P₂W₁₅**, resulting forming the POM organotin derivative based on trivalent Dawson moieties.

Cyclic voltammetry (CV). The electrochemistry of **SnR-Mn-P₂W₁₅** was determined in 1 mol L⁻¹ Na₂SO₄-H₂SO₄ aqueous solution (pH = 4.0) by CV. In the range of +0.2 to -1.0 V, the CV is restricted to the chemically reversible redox waves peaking at -0.391, -0.331 V (I-I'), -0.568, -0.502 V (II-II') and -0.858, -0.703 V (III-III'), with the peak potential separation (ΔE_p) of 0.060 V, 0.066 V and 0.155 V respectively (Fig. 4a). Comparing with the CVs of starting materials (see Fig. 4b,c), the obvious electrochemical response of W center was observed.¹⁹ Redox peaks I-I', II-II' and III-III' can be attributed to a one, one, two-electrons reversible redox process of W center, and the redox behaviors of Sn centers occur in the same I-I' region (Fig. 4c). While the Mn(II) being silent at our experimental conditions. A complementary cross-check of the stability of **SnR-Mn-P₂W₁₅** was detected by scan-cycling from 10 to 100 mV s⁻¹ (Fig. S9†). The peak potential is unchanged, which indicates the relatively high stability of **SnR-Mn-P₂W₁₅** under the given conditions.

30 Catalytic activities of **SnR-Mn-P₂W₁₅**

As shown in Fig. 5a, three well-defined redox couples can be observed in the solution of pH 4.0. **SnR-Mn-P₂W₁₅** shows a fine electrocatalytic activity towards the reduction of H₂O₂ as revealed by the changes in peak currents upon the addition of H₂O₂. With the continuous increase of the concentration of H₂O₂, the cathodic current increases, while the relative anodic current decreases. For comparison, the electrocatalytic activities of **Mn-P₂W₁₅** and MnCl₂ towards the reduction of H₂O₂ were also measured (Fig. S10†). The results show that **Mn-P₂W₁₅** and MnCl₂ also have certain electrocatalytic abilities on the reduction of H₂O₂, but the electrocatalytic activity of **SnR-Mn-P₂W₁₅** is significantly higher than those of MnCl₂ (Fig. S10b†) and the parent **Mn-P₂W₁₅** (Fig. S10c†).

In the process of electroreduction of nitrite, high overpotential was demanded in direct electroreduction, which was virtually impossible. POMs can lower the overpotential by delivering electrons to other species as a result of their capacity of storing massive electrons. Thus, the electrocatalytic reduction of NO₂⁻ by **SnR-Mn-P₂W₁₅** was studied. As shown in Fig. 5b, by the addition of NO₂⁻, the reduction peak current enhanced remarkably, while the corresponding oxidation peak current reduced. The outcome indicates that **SnR-Mn-P₂W₁₅** has a relatively excellent electrocatalytic activity for NO₂⁻ reduction. In addition, the catalytic activities of the related species were researched (Fig. S11). For **Mn-P₂W₁₅** and MnCl₂, their electrocatalytic activities for NO₂⁻ reduction are much lower compared with that of **SnR-Mn-P₂W₁₅** (see Fig. S11c†). **SnR-**

Mn-P₂W₁₅ can be used as relatively appropriate catalyst in electroreduction of nitrite as expected.

60 In multi-step organic synthesis of acid-catalytic protection for carbonyl group, an efficient and recoverable catalyst is indispensable and momentous. What is known to us is that ketone

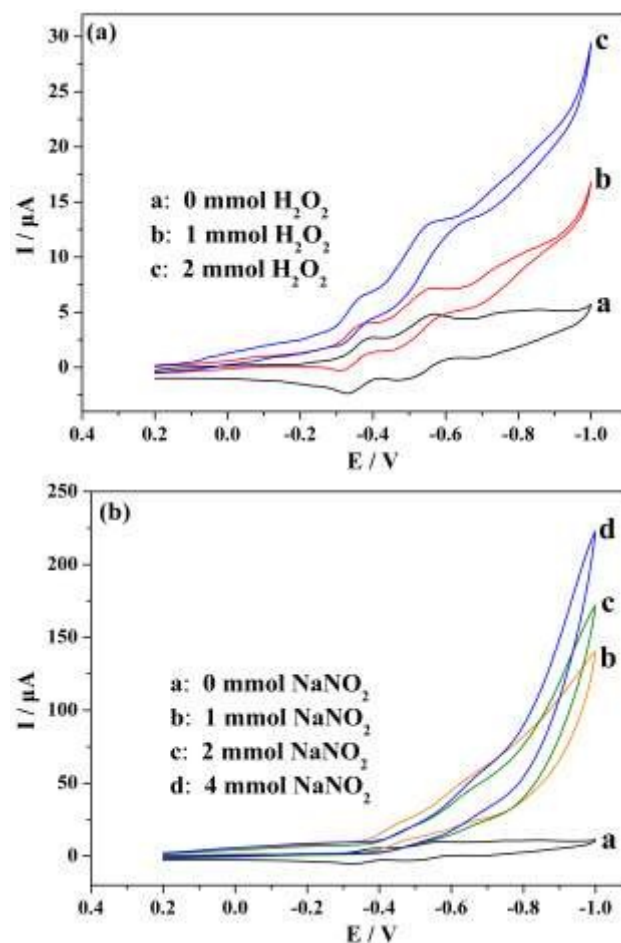


Fig. 5 Electrochemical reduction of (a) H₂O₂ and (b) NO₂⁻ with a 1.0 × 10⁻⁴ mol L⁻¹ solution of **SnR-Mn-P₂W₁₅** in a pH = 4 solution (1 mol L⁻¹ Na₂SO₄-H₂SO₄) at the scan rate of 50 mV s⁻¹, respectively.

reacts with an alcohol or glycol to form ketal in the presence of an acid catalyst (Scheme S2†). Therefore, we selected the synthesis of cyclohexanone ethylene ketal as a model reaction, to estimate the catalytic activities of **SnR-Mn-P₂W₁₅** and its parent compounds. In addition, the optimal reaction conditions, such as reaction time, molar ratio of starting materials and the amount of catalyst were also discussed systemically (Fig. S12-14†). Parallel experiments showed that the optimum conditions for the synthesis reaction of the cyclohexanone ethylene ketal were as follows: the cyclohexanone/glycol molar ratio of 1:1.4, 10 mL of cyclohexane (water-carrying agent), the catalyst (based on W)/cyclohexanone molar ratio of 1:200, 3.5 h and 95-100 °C. Furthermore, MnCl₂ and Cl₃SnCH₂CH₂COOCH₃ were also checked for comparison. From the results listed in Table S3,† it can be seen that the yields of ketal were 90, 10, 6, 86 and 97 % for **SnR-Mn-P₂W₁₅**, the parent **Mn-P₂W₁₅**, the monomer **P₂W₁₅**, MnCl₂ and Cl₃SnCH₂CH₂COOCH₃, respectively. Though Cl₃SnCH₂CH₂COOCH₃-catalyzed reaction harvested the highest ketal yield than other tested catalyst including **SnR-Mn-P₂W₁₅**,

the former was completely dissolved in the reaction mixture forming a homogenous system, while the latter was a heterogenous catalyst. Therefore, the as-synthesized **SnR-Mn-P₂W₁₅** can be recycled. To evaluate the reusability of our prepared compound, the **SnR-Mn-P₂W₁₅**-catalyzed reaction was performed for four cycles under the optimal reaction conditions (Fig. S15†). After each catalytic cycle, the catalyst was recovered by decantation without washing, and returned to subsequent cycles. The yield of cyclohexanone ethylene ketal shows a slight decrease during the first two cycles, which may be interpreted as the absorption of substrate (*e.g.* ethylene glycol or poly ethylene glycol) on the catalyst surface hindering the reactant contact with active sites. Nevertheless, the yields of ketal were keeping constant for the 3rd and 4th cycles.

Several mechanisms can be used to explain the acidity of polyoxometalates.²⁰ Degradation of saturated Dawson structure leads to the **P₂W₁₅** in alkaline environment, and the counter ion of Na⁺ displayed so weak Lewis acidity that made **P₂W₁₅** a undesirable candidate for an acid catalysis reaction. For the sandwich-type POM **Mn-P₂W₁₅**, the introduction of the transition metal made little contribution to its acid catalytic activity, which may be because of the full-coordination of Mn²⁺ in equatorial position even though two water molecules generate H⁺ by acid dissociation. Fortunately, organotin decorated **SnR-Mn-P₂W₁₅** expresses better catalytic effect may be owing to the Sn and Mn centers. Perhaps the four protons in the molecule also contribute to the acid catalysis. As seen in Table S3,† **Mn-P₂W₁₅** is insoluble in the reaction system, moreover, considering that Cl₃SnCH₂CH₂COOCH₃ and MnCl₂ are good homogenous acid catalysts, the new catalyst **SnR-Mn-P₂W₁₅** can be defined as a supported catalyst, in which POM moiety plays an important role like a “carrier” to decrease the solubility of catalyst in reaction mixture. Furthermore, the [C(NH₂)₃]⁺ guanidine cation, with a positive charge distributed in three N atoms and a C center, has a good thermal stability and a stronger electron-withdrawing effect,²¹ meanwhile exhibits Lewis acidity, so the Lewis acidity of the title compound increased. In fact, the determination of the active site for the ketalization needs to be further investigated.

Besides, the oxidative catalysis activity of **SnR-Mn-P₂W₁₅** was also evaluated. The effect of **SnR-Mn-P₂W₁₅** as a homogeneous catalyst in the oxidation of cyclohexanol to cyclohexanone was confirmed by selecting 30% H₂O₂ as an oxidant and acetonitrile as a solvent. At the selected reaction conditions according to the meticulous work reported in the literature,^{6c,22} the catalytic performances of several catalysts were investigated, and the results are listed in Table S4.† As seen from Table S4,† for TM/OM-containing catalysts **Mn-P₂W₁₅**, MnCl₂ and Cl₃SnCH₂CH₂COOCH₃, the isolated yields of the reaction are 16.7, 7.7 and 34.5%, respectively. The oxidative catalysis activities of them significantly reduced compared with that of **P₂W₁₅** (70.9% isolated yield of the product), which is probably due to their catalysis for the decomposition of hydrogen peroxide, and thus reducing the H₂O₂-dosage and contact time. **SnR-Mn-P₂W₁₅** exhibits better catalytic effect (72.4% isolated yield) in the for-mentioned available qualification than those of the parent materials. The results suggest that W(VI) is considered the active centers for the oxidative catalysis.

Conclusions

In this study, an unprecedented sandwich-type tungstophosphate based on trilacunary Dawson subunit was successfully synthesized by stepwise method in facile aqueous medium, which encapsulated transition metal manganese and organic metal organotin with outstretched carboxyethyl group in equatorial region. The synergistic effect between **P₂W₁₅** moieties and organotin [Sn(CH₂)₂COO]²⁺ groups results in good catalytic activities of acid-catalyzed in organic reaction. Our findings provided us with a chance to comprehend the step-by-step synthetic technique which can furnish an efficacious and feasible way for designing and constructing new polyoxometalate esterin derivatives with optimized functionality for future applications. Further exploration of photoelectrochemical properties of **SnR-Mn-P₂W₁₅** and preparation of new compounds are in progress, which will be reported in due course.

Acknowledgements

This work was financially supported by the Natural Science Foundation of Liaoning Province (no. 2013020128), the Foundation of Education Department of Liaoning Province (no. L2013414), the State Key Laboratory of Fine Chemicals of China (KF 1204) and the Key Laboratory of Polyoxometalate Science of Ministry of Education of China.

Notes and references

- ^a School of Chemistry and Chemical Engineering, Liaoning Normal University, Dalian 116029, China. E-mail: zhanglancai@lnnu.edu.cn; wsyu@lnnu.edu.cn; chemzhu@sina.com.
- ^b Center of Analytical Test, Liaoning Normal University, Dalian 116029.
- † Electronic Supplementary Information (ESI) available: ORTEP views and packing views of **SnR-Mn-P₂W₁₅**; Crystal structure figures, selected bond lengths and angles, IR spectra, TG curves, PXRD patterns, UV-visible spectra, CV curves, the optimal catalytic curves and other supplementary materials. CCDC 1045128 For ESI and crystallographic data in CIF or other electronic format. See DOI: 10.1039/b000000
- (a) L. Li, J. W. Sun, J. Q. Sha, G. M. Li, P. F. Yan, C. Wang and L. Yu, *Dalton Trans.*, 2015, **44**, 1948; (b) Y. Wang, X. P. Sun, S. Z. Li, P. T. Ma, J. P. Wang and J. Y. Niu, *Dalton Trans.*, 2015, **44**, 733; (c) X. L. Wang, N. Li, A. X. Tian, J. Ying, T. J. Li, X. L. Lin, J. Luan, and Y. Yang, *Inorg. Chem.*, 2014, **53**, 7118; (d) X. J. Sang, J. S. Li, L. C. Zhang, Z. J. Wang, W. L. Chen, Z. M. Zhu, Z. M. Su and E. B. Wang, *ACS Appl. Mater. Interfaces*, 2014, **6**, 7876; (e) A. Sap, G. Absillis and T. N. Parac-Vogt, *Dalton Trans.*, 2015, **44**, 1539; (f) L. D. Matteis, S. G. Mitchell and J. M. de la Fuente, *J. Mater. Chem. B.*, 2014, **2**, 7114; (g) M. K. Saini, R. Gupta, S. Parbhakar, S. Singh and F. Hussain, *RSC Adv.*, 2014, **4**, 38446; (h) W. J. Liu, J. H. Christian, R. Al-Oweini, B. S. Bassil, J. V. Tol, M. Atanasov, F. Neese, N. S. Dalal and U. Kortz, *Inorg. Chem.*, 2014, **53**, 9274; (i) M. P. Santoni, A. K. Pal, G. S. Hanan, M. C. Tang, A. Furtos and B. Hasenknopf, *Dalton Trans.*, 2014, **43**, 6990.
- (a) L. Ruhlmann, D. Schaming, I. Ahmed, A. Courville, J. Canny and R. Thouvenot, *Inorg. Chem.*, 2012, **51**, 8202; (b) C. Lydon, C. Busche, H. N. Miras, A. Delf, D. L. Long, L. Yellowlees, and L. Cronin, *Angew. Chem. Int. Ed.*, 2012, **51**, 2115; (c) F. Doungmene, P. A. Aparicio, J. Ntienoue, C. S. A. Mezui, P. D. Oliveira, X. López and I. M. Mbomekallé, *Electrochim. Acta*, 2014, **125**, 674; (d) C. C. Zhao, E. N. Glass, B. Chica, D. G. Musaeu, J. M. Sumliner, R. B. Dyer, T. Q. Lian and C. L. Hill, *J. Am. Chem. Soc.*, 2014, **136**, 12085; (e) P. E. Car, M. Guttentag, K. K. Baldrige, R. Alberto and G. R. Patzke, *Green Chem.*, 2012, **14**, 1680.
- F. B. Xin, M. T. Pope, *Organomet.*, 1994, **13**, 4881.

4. (a) L. Liu, L. Hu, Q. Liu, Z. L. Du, F. B. Li, G. H. Li, X. J. Zhu, W. Y. Wong, L. Wang and H. Li, *Dalton Trans.*, 2015, **44**, 306; (b) B. X. Dong, L. Chen, S. Y. Zhang, J. Ge, L. Song, H. Tian, Y. L. Teng and W. L. Liu, *Dalton Trans.*, 2015, **44**, 1435; (c) J. H. Qiu, X. Y. Zhou, Q. Q. Mo, F. Liu and L. P. Jiang, *RSC Adv.*, 2014, **4**, 48931; (d) H. J. Lv, W. W. Guo, K. F. Wu, Z. Y. Chen, J. Bacsá, D. G. Musaev, Y. V. Geletii, S. M. Lauinger, T. Q. Lian and C. L. Hill, *J. Am. Chem. Soc.*, 2014, **136**, 14015; (e) L. Zhang, W. B. Yang, X. F. Kuang, X. Y. Wu and C. Z. Lu, *Dalton Trans.*, 2014, **43**, 16328; (f) W. C. Chen, L. K. Yan, C. X. Wu, X. L. Wang, K. Z. Shao, Z. M. Su and E. B. Wang, *Cryst. Growth Des.*, 2014, **14**, 5099; (g) A. X. Tian, X. Hou, N. Sun, R. Xiao, J. Ying, Y. Yang, Y. L. Ning, T. J. Li and X. L. Wang, *Z. Anorg. Allg. Chem.*, 2014, **640**, 2968;
5. (a) S. Bareyt, S. Piligkos, B. Hasenknopf, P. Gouzerh, E. Lacôte, S. Thorimbert and M. Malacria, *J. Am. Chem. Soc.*, 2005, **127**, 6788; (b) C. Boglio, K. Micoine, É. Derat, R. Thouvenot, B. Hasenknopf, S. Thorimbert, E. Lacôte and M. Malacria, *J. Am. Chem. Soc.*, 2008, **130**, 4553; (c) L. C. Zhang, S. L. Zheng, H. Xue, Z. M. Zhu, W. S. You, Y. G. Li and E. B. Wang, *Dalton Trans.*, 2010, **39**, 3369; (d) C. Brazel, N. Dupré, M. Malacria, B. Hasenknopf, E. Lacôte and S. Thorimbert, *Chem. Eur. J.*, 2014, **20**, 16074.
6. (a) L. C. Zhang, H. Xue, Z. M. Zhu, Q. X. Wang, W. S. You, Y. G. Li and E. B. Wang, *Inorg. Chem. Commun.*, 2010, **13**, 609; (b) Z. J. Wang, L. C. Zhang, Z. M. Zhu, W. L. Chen, W. S. You and E. B. Wang, *Inorg. Chem. Commun.*, 2012, **17**, 151; (c) H. Yang, L. C. Zhang, L. Yang, X. L. Zhang, W. S. You and Z. M. Zhu, *Inorg. Chem. Commun.*, 2013, **29**, 33; (d) X. J. Sang, J. S. Li, L. C. Zhang, Z. M. Zhu, W. L. Chen, Y. G. Li, Z. M. Su and E. B. Wang, *Chem. Commun.*, 2014, **50**, 14678.
7. (a) K. Sakamoto, Y. Hamada, H. Akashi, A. Orita and J. Otera, *Organomet.*, 1999, **18**, 3555; (b) S. Durand, K. Sakamoto, T. Fukuyama, A. Orita, J. Otera, A. Duthie, D. Dakternieks, M. Schulte and K. Jurkschat, *Organomet.*, 2000, **19**, 3220; (c) J. Cervantes, R. Zárraga and C. S. Hernández, *Appl. Organomet. Chem.*, 2012, **26**, 157.
8. (a) T. T. Yu, H. Y. Ma, C. J. Zhang, H. J. Pang, S. B. Li and H. Liu, *Dalton Trans.*, 2013, **42**, 16328; (b) C. N. Kato, T. Kashiwagi, W. Unno, M. Nakagawa and H. Uno, *Inorg. Chem.*, 2014, **53**, 4824; (c) C. Lydon, M. M. Sabi, M. D. Symes, D. L. Long, M. Murrie, S. Yoshii, H. Nojiri and L. Cronin, *Chem. Commun.*, 2012, **48**, 9819.
9. (a) R. G. Finke, M. W. Droegge and P. J. Domaille, *Inorg. Chem.*, 1987, **26**, 3886; (b) C. J. Gómez-García, J. J. Borrás-Almenar, E. Coronado and L. Ouahab, *Inorg. Chem.*, 1994, **33**, 4016.
10. R. E. Hutton, J. W. Burley and V. Oakes, *J. Organomet. Chem.*, 1978, **156**, 369.
11. (a) G. M. Sheldrick, *SHELXL97, program for crystal structure refinement*, University of Gottingen, Germany, 1997; (b) G. M. Sheldrick, *SHELXS97, program for crystal structure solution*, University of Gottingen, Germany, 1997.
12. (a) I. D. Brown and D. Altermatt, *Acta Crystallogr. Sect. B: Struct. Sci.*, 1985, **41**, 244; (b) H. H. Thorp, *Inorg. Chem.*, 1992, **31**, 1585.
13. (a) S. Yao, J. H. Yan, Y. C. Yu and E. B. Wang, *J. Coord. Chem.*, 2012, **65**, 1451; (b) M. K. Rauf, M. A. Saeed, I.-u. Din, M. Bolte, A. Badshah and B. Mirza, *J. Organomet. Chem.*, 2008, **693**, 3043.
14. J. W. Zhao, J. Zhang, Y. Song, S. T. Zheng and G. Y. Yang, *Eur. J. Inorg. Chem.*, 2008, **2008**, 3809.
15. Y. Y. Zheng, R. Wen, X. J. Kong, L. S. Long, R. B. Huang and L. S. Zheng, *Dalton Trans.*, 2012, **41**, 9871.
16. X. Tong, X. F. Wu, Q. Y. Wu, W. M. Zhu, F. H. Cao and W. F. Yan, *Dalton Trans.*, 2012, **41**, 9893.
17. I. Ahmed, R. Farha, Z. H. Huo, C. Allain, X. X. Wang, H. L. Xu, M. Goldmann, B. Hasenknopf and L. Ruhlmann, *Electrochim. Acta.*, 2013, **110**, 726.
18. (a) D. K. Lyon, W. K. Miller, T. Novet, P. J. Domaille, E. Evitt, D. C. Johnson and R. G. Fink, *J. Am. Chem. Soc.*, 1991, **113**, 7209; (b) X. Zhang, Q. Chen, D. C. Duncan, R. J. Lachicotte and C. L. Hill, *Inorg. Chem.*, 1997, **36**, 4381; (c) T. L. Jorris, M. Kozik, N. Casan-Pastor, P. J. Domaille, R. G. Finke, W. K. Miller and L. C. W. Baker, *J. Am. Chem. Soc.*, 1987, **109**, 7402.
19. (a) N. Fay, E. Dempsey and T. J. McCormac, *J. Electroanal. Chem.*, 2005, **574**, 359; (b) X. G. Cao, L. W. He, B. Z. Lin, Z. J. Chen and P. D. Liu, *Inorg. Chim. Acta.*, 2009, **362**, 2505.
20. (a) C. Boglio, G. Lemièrre, B. Hasenknopf, S. Thorimbert, E. Lacôte and M. Malacria, *Angew. Chem. Int. Ed.*, 2006, **45**, 3324; (b) B. Riflade, D. Lachkar, J. Oble, J. Li, S. Thorimbert, B. Hasenknopf and E. Lacôte, *Org. Lett.*, 2014, **16**, 3860.
21. P. Gros, P. L. Perchec and J. P. Senet, *J. Org. Chem.*, 1994, **59**, 4925.
22. C. Y. Yang, L. C. Zhang, Z. J. Wang, L. Wang, X. H. Li and Z. M. Zhu, *J. Solid. State Chem.*, 2012, **194**, 270.